Title	The internal structure of a rockslide dam induced by the 2008 Wenchuan (Mw7.9) earthquake, China
Author(s)	Wang, Gonghui; Huang, Runqiu; Kamai, Toshitaka; Zhang, Fanyu
Citation	Engineering Geology (2013), 156: 28-36
Issue Date	2013-04
URL	http://hdl.handle.net/2433/173357
Right	© 2013 Elsevier B.V.
Type	Journal Article
Textversion	author

1   September 24, 2012

2   Submitted to *Engineering Geology*

3

4   Title:

5   The internal structure of a rockslide dam induced by the 2008 Wenchuan (M_w7.9) earthquake, China

6

7   Authors: Gonghui Wang, Runqiu Huang, Toshitaka Kamai, Fanyu Zhang

8

9   **Addresses of authors:**

10   Gonghui Wang, Assistant Professor (Corresponding author)

11   Research Center on Landslides

12   Disaster Prevention Research Institute

13   Kyoto University

14   Gokasho, Uji, 611-0011

15   Japan

16   Tel: (+81)774-384114; Fax:(+81)774-384300

17   e-mail: wanggh@landslide.dpri.kyoto-u.ac.jp

18

19   Runqiu Huang, Professor

20   State Key Laboratory of Geo-hazard Prevention and Geo-environment Protection

21   Chengdu University of Technology

22   Chengdu, Sichuan 610059

23   P.R. China

24

25   Toshitaka Kamai, Professor

26   Disaster Prevention Research Institute

27   Kyoto University

28   Gokasho, Uji, 611-0011

29   Japan

30

31   Fanyu Zhang, Dr.

32   Disaster Prevention Research Institute, Kyoto University, Japan

33   (Currently, School of Civil Engineering and Mechanics, Lanzhou University, Lanzhou, Gansu, P.R. China)

34   Abstract:

35   The internal structure of landslide dams plays a key role in their stability; however, it has not been much studied,

36   probably due to the difficulty in obtaining information on internal structure in most cases. Here, we examined the

37   shear-wave-velocity structure of a rockslide dam by a surface-wave technique called multichannel analysis of

38   surface waves (MASW). During the 2008 Wenchuan earthquake (M_w7.9), more than 60,000 landslides were

39   triggered and 800 landslide dams formed. Those dams with a high risk of collapse threatened rescue activities,

40   and almost all of the large landslide dams were treated by digging a sluiceway immediately after the earthquake.

41   Although the risk of collapse of many landslide dams was removed or lowered, not all of the countermeasures

42   were based on well controlled methods. To analyze the internal of landslide dams to assist in carrying out

43   reliable countermeasures, we made detailed investigations on some of the dams, and here describe one landslide

44   dam that occurred in the Tianchi area. Grain-size analysis revealed that the displaced landslide materials

45   experienced fragmentation and segregation during the long movement. The shear-wave-velocity profile of the

46   dam revealed that the dam consisted of three facies (carapace, body and basal facies). The boundary between

47   facies is distinct. The body facies had a greater shear-wave velocity (compared to those landside dams that had

48   suffered collapse failure during the construction of a sluiceway), showing that the dam consisted of more densely

49   deposited materials. This kind of dam body had a lower permeability, capable of retarding seepage that triggers

50   collapse failure of the dam body due to piping. Big blocks on the surface also enabled the dam body to have

51   greater resistance to overflow and thus reducing possible collapse failure in the immediate aftermath of

52   overtopping.

53

54   Key Words: Landslide dam, 2008 Wenchuan earthquake, internal structure, stability of landslide dam, grain size

55   distribution

56

57   Introduction

58   Landslide dams form when large landslides block river flows, forming lakes. Landslide dams formed by

59   such mass movements are often weak in structure, and can fail under their own weight or by overtopping.

60   Sometimes the released water carrying landslide debris causes fatalities and substantial damage to properties

61   downstream. For example, a landslide dammed Dadu River in an earthquake in Sichuan Province in 1786. Ten

62   days later, the dam failed, resulting in a devastating flood that reached 1400 km downstream, killing about

63   100,000 people (Li et al., 1986).

64   In recent years, many landslide dams triggered by earthquakes and rainfall have been reported. They often

65   cause great difficulties to the recovery phases in the hazard areas, and also threaten the safety of people living

66   downstream. It is normally required to make a risk assessment of the stability of the dam within a short time

67   immediately after the dam's formation (Tabatake et al. 2002). Two different approaches, the topographical

68   approach (Costa & Schuster 1988, 1991; Casagli & Ermini 1999; Ermini & Casagli, 2003; Korup, 2002, 2004)

69   and the hydraulic approach (Mizuyama et al, 1987, 1989; Takahashi and Kuang, 1988; Takahashi and Nakagawa,

70   1993), have been developed to analyze the possible longevity of the dam and the flood profile when the dam is

71   breached. The topographical characteristics and the breaching failure mechanisms due to overtopping have been

72   widely examined. Nevertheless, our understanding of the formation of landslide dams is still poor; so many

73   countermeasures for dealing with some giant landslide dams are empirically based. Normally, a landslide dam

74   consists of heterogeneous displaced debris, with properties determined by the locality as well as by the

75   movement of the landslide itself. Hence, in many cases, although the risk of dam breaching has been

76   acknowledged and understood, there are still cases in which the dam has collapsed while countermeasures were

77   being carried out. For example, in 2000, a giant rock avalanche formed a large landslide dam in the Yigong area,

78   Tibet, China, and the main countermeasure was digging a sluiceway. However, the dam collapsed suddenly after

79   the sluiceway was finished, resulting in severe downstream flooding, killing about 100 people downstream, and

80   resulting in 5,000 people losing their homes (Zhu et al., 2003). Although this kind of catastrophic failure had

81   occurred previously, the countermeasures for the Tangjiashan landslide dam formed in the 2008 Wenchuan

82 earthquake in Sichuan, China (dam height: about 100 m; dam volume: about 24 Mm^3; storage capacity of

83 dammed lake: about 320 Mm^3) was also the construction of a spillway across the dam. Abrupt breaching

84 occurred due to rapid erosion at the dam site, and a great flood threatened the cities downstream, such as

85 Beichuan and Mianyang (Liu et al., 2009). Fortunately, only 1/3 of the dam height was breached, and 2/3 of the

86 dam height remained stable, preventing the release of the entire reservoir of water. On the other hand, some

87 hundreds of tonnes of dynamite were used on another landslide dam (formed during the 2008 Wenchuan

88 earthquake), in an attempt to make a spillway by blasting to lower the risk of an outburst flood in case the dam

89 breached abruptly. However, the explosion only functioned to break the big rocks, and the landslide dam itself

90 was stable enough. From these cases, we can conclude that a proper approach for analyzing whether a landslide

91 dam is stable or not has not been set up from an engineering viewpoint.

92   During the 2008 Wenchuan (M_w7.9) earthquake, more than 90,000 people were killed due to the collapse of

93 houses or landslides. The earthquake triggered 40 − 60 thousand landslides (Huang, 2009; Dai et al., 2011;

94 Gorum et al., 2011) and more than 800 landslide dams were formed (Fan et al., 2012), greatly hindering recovery

95 and reconstruction in the seismic hazard area. Almost all of the landslide dams failed naturally or were removed

96 artificially soon after the earthquake. However, some of the larger landslide dams still remain, impounding large

97 volumes of water, so there is still a major risk of outburst flooding. Therefore, it is of great importance to

98 develop a fast and effective method to assess the risk of outburst flooding due to landslide dam failure.

99   To assist in assessing the risk of outburst flooding due to landslide dam failure, we carried out detailed field

100 surveys of some of the big landslide dams formed during the 2008 Wenchuan earthquake, investigating the

101 geological and topographical characteristics of the landslides, their processes of formation and the internal

102 structure of the landslide dams. In this paper, through study of the landslide dam formed in Tianchi Town,

103 Mianzhu City, we examine the formation of a landslide dam resulting from a long-travel rockslide occurring in a

104 carbonate rock area. We surveyed the internal structure of the dam site by means of a multiple-channel

105 surface-wave technique, and also analyzed the grain size distribution at the dam site. Based on the survey results,

106 we discuss the dam's formation and stability. Fig. 1 shows the epicenter the 2008 Wenchuan earthquake, the

107   locations of landslides and the location of the Tianchi landslide dam.

108

109   **2. Wenchuan earthquake and landslide dams**

110   On May 12, 2008, at 14:28 hr local time, an earthquake (M_w7.9), with a hypocentre at 30.99°N, 103.36°E,

111   at a depth of 19 km occurred in Sichuan province, China (USGS, 2008). This is known as the Wenchuan

112   earthquake, named after the earthquake's epicenter in Wenchuan County (Fig. 1). The maximum ground

113   acceleration recorded during the earthquake was at Wolong, 18 km WNW of the epicenter. Peak accelerations

114   there were 957.7 gal in the East-West direction, 652.9 gal in the North-South direction, and 948.1 gal vertically

115   (Li *et al*., 2008). The earthquake was felt as far away as Beijing (1500 km away) and Shanghai (1700 km away),

116   and also in some nearby countries. Strong aftershocks continued to hit the area months after the main quake,

117   causing further casualties and damage.

118   The 2008 Wenchuan earthquake occurred in the Longmen Shan thrust zone, which is located on the eastern

119   boundary area of the Tibetan plateau. The Longmen Shan thrust zone is one of the most significantly deformed

120   regions in China, with many seismically active faults (Burchfiel *et al*., 1995, 2008; Jia *et al*., 2006, 2007;

121   Densmore *et al*., 2007). The thrust zone is about 60 km wide, and marks the topographic boundary between the

122   eastern Tibetan Plateau and the Sichuan basin. The convergence rate across the thrust zone is inferred to be 4-6

123   mm/yr (Deng *et al*., 1994). Earthquakes occur frequently along this zone. In 1933, a M7.5 earthquake occurred

124   in Diexi, 50 km northeast of Wenchuan. During this earthquake, some large lakes were formed behind landslide

125   dams, and 6800 people were killed (about 2500 people were directly killed by the floods that followed collapse

126   of two landslide dams). In 1976, two earthquakes (M7.2) occurred in Songpan and Pingwu, northeast of

127   Chengdu.

128   In the Wenchuan earthquake area, the rocks in the vicinity of the Longmen Shan thrust zone are mainly

129   composed of Triassic granite, metamorphosed sandstone, phyllite, sandy slate and dolomite (Ma, 2002). The

130   rocks are closely jointed due to strong tectonic movement in this area. The adjacent Chengdu basin has been less

131   affected by tectonic activity and remained relatively stable throughout the Cenozoic; here the strata of Jurassic

132   and Cretaceous age are covered by Quaternary alluvium (Ma, 2002).

133   The earthquake formed more than 800 landslide dams (Fan et al., 2012), of which 104 had heights of >10 m,

134   impounding >10,000 m^3 of water, and with catchment areas >20 km^2. Based on the scale of the landslide dam,

135   the possible peak value of outburst flooding after breaching, and the possible downstream flooding area, the

136   degree of risk of each landslide dam was placed into one of three risk categories (high, medium and low). Of the

137   landslide dams, 6 were at high risk, 25 were at medium risk and 72 were at low risk (Liu, 2008; Yin, 2008).

138   Emergency treatment measures had been carried on many of the landslide dams. The emergency work on the

139   Tangjiashan landslide dam was reported worldwide and attracted wide concern.

140

141   3. Landslide dam in the Tianchi area

142   The landslide dam in Tianchi town (hereinafter called the Tianchi landslide dam) (Fig. 2), about 100 km

143   north of Chengdu, resulted from a rock avalanche occurring on the right slope of a tributary of the Mianyuan

144   River in Mianzhu City. Fig. 2a shows a satellite image of the landslide area taken before the earthquake. Figs. 2b

145   and 2c present an oblique view of the whole dam site and a view from upstream. Fig. 2d shows a view of the

146   dam from downstream, in which the piping is marked by a circle. From the Google Earth image and field

147   investigation, we inferred that there was an unstable rock at the source area before the earthquake (marked as

148   'Unstable block' in Fig. 2a). The geological setting of the Tianchi area is presented in Fig. 3. The landslide area

149   consists of Devonian clastics and carbonate (dolomite or dolomitic limestone). Bedding planes and joints of the

150   bed rock in the source area were surveyed and are shown in Fig. 4, and they can be mainly divided into 5 groups.

151   The bedrock of the source area was fractured by these bedding planes and joints, and a big unstable wedge was

152   formed on the bedrock near the mountain ridge (Fig.4a). This unstable wedge failed during the earthquake, and

153   traveled downslope rapidly (~28.5 m/s, Wang et al., 2011), burying the river channel, and climbing the slope of

154   the opposite bank. A landslide dam was formed, with a dam height of 34–41 m, a length (along the river channel)

155   of 158 m, and a width (across the river channel) of 70–102 m. The city hall, elementary school, and some houses

156   on the upstream side were flooded by the impounded water. Fig. 5 shows the cross section along line I-I' shown

157   in Fig. 2a. For the cross section in Fig. 5, the topography after the quake was measured by a laser measuring

158   technique (Trupulse360), while the topography before the quake was inferred from maps and field investigation.

159   The landslide dam is located on a tributary of the Miyuan River. The local engineers thought that the

160   landslide dam was formed by big rock blocks, because the surface is covered by big rocks up to 6 m. Water

161   flows from the lower part of the landslide dam on the downstream side, and the water level of the barrier lake

162   was almost constant.

163   No engineering work was undertaken on the Tianchi landslide dam for about one and half years after the

164   earthquake. Thereafter, following the need for recovery and reconstruction work upstream of the landslide dam,

165   a spillway was dug in the dam gradually by steps. Finally, the dam was excavated to the level of the river bed

166   before the earthquake. Fig. 6 shows the status of excavation of the channel at different times (Fig.6a on June,

167   2010). The channel had been excavated in three steps at the time of our first survey, and had reached the original

168   bed river at the time of our second survey (June, 2010). The progressive channel excavation enabled us to

169   perform a geophysical survey using a surface wave technique called the multichannel analysis of surface waves

170   (MASW) and also carry out grain-size-distribution analysis of the soil layers in the dam at different depths.

171

172   **4 Internal structure of the landslide dam**

173   4.1 Grain-size distribution

174   The surface of Tianchi landslide dam was almost completely covered by very large boulders (c. 2–6 m in

175   diameter). Observations of the soil layers in the dam exposed as channel construction progressed revealed that

176   the boulders were mostly in the surficial soil layer; immediately below the surficial layer were small boulders (<

177   0.5 m), gravels and finer debris. To analyze the grain-size distribution of soil layers at different depths within the

178   dam, we analyzed grain size by sieving and photography. The reliability of this combined method for grain size

179   distribution analysis has been verified by Casagli et al (2003). We performed the analysis by following steps.

180   (1) The area ratio of grains with $\varphi > 40$mm was measured by means of particle digital image analysis. Due to

181   the progressive excavation of the channel, soil layers at different depths were exposed. We sampled 11 points at

182   different soil layer levels, reshaping the face locally to be vertical. Two orthogonally oriented scales were put on

183   the vertical surface, and photographs were taken.

184   (2) For the target measuring area, the area ratios of grains with differing sizes were calculated by

185   photographic analysis. After taking the photo, the grain in each photograph was outlined by drawing a line along

186   its boundary. Using the outlined figure, the diameter (the diameter of the inscribing cycle of the outline) and the

187   cross section area of each grain were calculated, and the total cross section area of grains with the same diameter

188   was then calculated. Considering the possibility of human error in drawing the outlines of grains, we used a

189   photographic analysis method to analyze the larger grains with $\varphi > 4.75$mm.

190   (3) We took samples from the surface of the photographed area, sieved out those gravels with $\varphi > 50$ mm,

191   and took 10 kg of samples ($\varphi \leq 50$ mm) to the laboratory for further grain size analysis by sieving following the

192   ASTM standard.

193   (4) The percentages of grains with different grain sizes were calculated. Assuming that the debris has the

194   same density, the percentages by weight of grains with differing sizes were calculated through the area ratio

195   (obtained by particle digital image analysis) of different grains and the results from sieving analysis.

196   We sampled 11 locations for the distribution of grain size in the Tianchi landslide dam (Fig. 6a). Samples

197   P1 – P8 were taken on November 2009, and P9 – P11 on June 2012. P1 – P4 and P8 are located on the upper

198   steps along the road, P5 – P7 are on the side slope of the excavation at level L3. P9 – P11 are located at the

199   bottom of the excavation (about 2 m above the outcropping former river bed). P9 is near the downstream margin

200   of the landslide dam, while P10 is below P7, and P11 is below P5. Fig. 7 presents the grain-size distributions.

201   Because very large boulders were located only in the surficial layer, there were no grains >50cm in Fig. 7. From

202   the grain size distribution of P1 – P4, and P8 (Fig. 7a), we saw that the grains tended to become coarser closer to

203   the lateral margins (say, P8 and P9). This tendency is normal in the deposits of large-scale rock avalanches

204   (Schulz et al., 2008; Crosta et al., 2011; Davis and McSaveney, 2011; Dunning and Armitage 2011), due to the

205   segregation of grains during movement. Nevertheless, a similar tendency was missing in the grain-size

206   distribution of P5 – P7 (Fig. 7b). This may result from the facts that P5 – P7 were located in the deeper soil

207   layers of the dam site, and the distance between them was relatively short.

208

209   4.2 Shear-wave velocity profile of the landslide dam

210   To investigate the internal structure of the landslide dam, we used a surface-wave method known as

211   multichannel analysis of surface waves (MASW) (Park et al., 1999; Hayashi and Suzuki, 2004) to measure the

212   shear-wave velocity profile of the landslide-dam site. The survey principle of MASW and the layout of

213   equipment (Seismograph: Model McSEIS-SXW, OYO Corporation, Tokyo, Japan; Geophones: Model GS-11D,

214   OYO Geospace Corporation, Houston, Texas, USA) are outlined in Fig. 8. In the survey, 24 geophones were

215   spaced at 2 m intervals along a line. A wooden hammer (about 8 kg) was used as the seismic motion exciter. The

216   hammer points were outside of both ends of the survey line and also intermediate between the geophones. We

217   carried out our first survey in November 2009, when the landside dam had been excavated with the shape shown

218   in Fig. 6b. The landslide dam excavation had three steps (L1, L2 and L3), with the most upper one (L1) along the

219   original road before the earthquake and exposed during the excavation. Step L3 (shown by dashed line) was flat

220   at the time of our survey, although it was later dug deeper as excavation progressed. In June of 2010, we

221   surveyed this area again, when the excavation had been finished, and the bottom of the excavation had reached

222   almost to the original river bed level (L4). Hereinafter, we call these survey lines L1, L2, L3, and L4,

223   respectively. Fig. 9 show the shear-wave velocity profile along survey line L1, and Fig.10 along survey lines L2

224   to L4. As mentioned above, L1 is along the original road. The shear-wave velocity values obtained along this

225   line thus represent those of the slope before the earthquake. As shown in Fig. 9, most of the field has shear-wave

226   velocity values ranging from 400–480 m/s. However, around 30 m from the beginning point and at a depth of 9

227   m, shear-wave velocity values are smaller (ranging from 350–400m/s). This field of smaller shear-wave velocity

228   values might reflect the former channel of the stream, i.e., landslide debris buried the stream path, with the soil

229   layer deposited being looser than the surrounding original mountain slope.

230   Survey line L2 was along the newly built road. Due to the construction of the road, a 3–5m thick soil layer

231   had been excavated (Fig. 6b). In L2, the whole surficial layer (about 6 m deep) and all soil layers (from the

232   surface to the bottom) 0–30 m from the upstream end of the line had relatively smaller shear-wave velocity

233   values (330–390 m/s) (Fig. 10a). Most of the soil layer along L3 showed greater shear-wave velocity values (400

234   m/s–480 m/s) (Fig. 10b). However, the domain on the middle part of the survey line (30–60m) and 7–10m deep

235   had relatively smaller shear-wave velocity values (330m/s–400m/s). Although the grain size of the soil layer near

236   this area was not measured, from the grain size distribution of the surficial soil layers in L3 (P5–P7 in Fig. 7b),

237   we can infer that the effective grain size (D_{10}) tended to become smaller. If it is assumed that the soil density is

238   everywhere constant, the rigidity modulus becomes smaller with decrease of gravel content. Because the

239   shear-wave velocity $V_s = \overline{\quad}$ (G: Rigidity modulus; ρ: mass of soil layer), the smaller the rigidity modulus is,

240   the smaller the shear-wave velocity becomes. Therefore, we infer that the area with smaller shear-wave velocity

241   (shown in the ellipsoidal area) might result from a segregation phenomenon as shown in Fig. 7. Due to the

242   segregation process during movement, finer debris accumulated in this area, forming soil layers that are

243   relatively weaker than the surrounding domain. The soil layer below line L4 showed high shear-wave velocity

244   values (400 m/s–480 m/s) in general, with a small area with relative low shear-wave velocities (330–390 m/s).

245   However, the soil layer near the bottom (the original river bed) showed lower shear-wave velocities

246   (250–300m/s). This may partially result from the original fluvial river-channel deposits and also the entrained

247   substrate mixed with rockslide debris.

248

249   **5. Discussion**

250   It has been noted that breaching of landslide dams normally results from three types of failure processes

251   (Takahashi and Kuang, 1988), i.e., overtopping erosion, occurrence of slides on the whole dam, and progressive

252   failure. It has also been noted that overtopping breaching is dominant in breached landslide dams, and that

253   progressive dam failure due to seepage (piping flow) is rare (Mizuyama et al., 1987, 1989). However, of the 32

254   big landslide dams that formed during the 2008 Wenchuan (M_w7.9) earthquake and had engineered channels

255   excavated in them, 8 failed from piping flow (Xu et al. 2009). Thus, in the case of the Wenchuan earthquake,

256   piping-triggered catastrophic breaching of landslide dam was not rare. Furthermore, many of the landslide dams

257   that consisted of finer grained debris of sand and gravels suffered breaching due to overtopping erosion. On the

258   other hand, landslide dams consisting of coarser materials (such as gravels and huge boulders) showed greater

259   stability (Chigira et al., 2010; Wang, 2011).

260   For longevity analysis of landslide dams, an approach termed the *Dimensionless Blockage Index* (*DBI*) has

261   been proposed by Ermini and Casagli (2003).

262         $DBI = \log (A_b \quad H_d/V_d)$ (1)

263   where A_b is area of the catchment (km^2); H_d is height of the landslide dam (m) ; V_d is volume of the landslide

264   dam ($\times 10^6$ m^3). Based on the analysis of many recorded landslide dams all over the world, Ermini and Casagli

265   (2003) recognized three "stability domains" for the dimensionless blockage index (1) when $DBI<2.75$, the

266   landslide dam lies in the stability domain; (2) when $2.75<DBI<3.08$, the landslide dam is in the uncertain

267   domain; and (3) when $DBI > 3.08$, the landslide dam is in the instability domain.

268   For Tianchi landslide dam, its length is about 158 m, width 70–102 m, and height 34–41 m, the upstream

269   catchment area is about 30.83 km^2. Equation 1 indicated a *Dimensionless Blockage Index* value of 3.72. Hence,

270   Tianchi landslide dam could be regarded to lie in the instability domain. However, no breaching occurred before

271   the channel was excavated. This suggested that the landslide dam itself was stable. It is noted that during the

272   channel excavation on some other large landslide dams formed in the same earthquake in Sichuan, such as

273   Tangjiashan, Xiaojiaqiao, and Xiaogangjian, etc, abrupt dam breaching occurred, resulting in catastrophic

274   flooding downstream. In Fig. 11, we superimposed the plot of catchment area against V_d/H_d together with those

275   obtained by Ermini & Casagli (2003), where SD means the stability domain, UD instability domain. The risk of

276   abrupt breaching of some large landslide dams formed in the 2008 Wenchuan earthquake is correctly indicated

277   by the Dimensionless Blockage Index, with the exception of the Tianchi landslide dam. This may be due to the

278   fact that the Dimensionless Blockage Index is based on topographic features of the landslide dam and the

279   upstream catchment area, without consideration of the dam's geotechnical properties. Such anomalous behavior

280   has also been reported by Strom (2010), who suggests that additional quantitative parameters characterizing

281   landslide dams and dammed lakes should be used in the stability analysis of landslide dams. However, although

282   the geotechnical properties of landslide dams play a key role in dam stability and also in the resistance to

283   overtopping erosion, they have been rarely incorporated before now, probably due to the difficulties in obtaining

284   them.

285   We surveyed the shear-wave velocity profiles of several large landslide dams formed in the 2008 Wenchuan

286   earthquake, and found that those dams that abruptly breached during the construction of the sluiceway had

287   shear-wave velocity values smaller than 250 m/s (Wang, 2011). It is known that the standard penetration test N

288   value of a soil layer has a positive correlation with the shear-wave velocity (Imai and Tonouchi, 1982). A higher

289   shear-wave velocity value means that the soil layer has greater penetration resistance, indicating that the soil

290   layer is more tightly consolidated. From Fig. 10 we can see that almost all the domains of Tianchi landslide dam

291   have greater shear-wave velocity values (say, >300 m/s). Therefore, we conclude that the landslide dam is in a

292   tightly consolidated state, so no abrupt breaching could occur during the discharge of impounded water after the

293   channel excavation was finished. The greater shear-wave velocities may be due to the fact that the landslide

294   debris with high mobility rushed into the river valley, and was deposited there suddenly, leading to the debris

295   being tightly consolidated. Such tightly consolidated landslide dams may be less likely to experience slides

296   compared to loosely deposited landslide dams (Foster et al., 2000).

297   According to Dunning and Armitage (2011), rock-avalanche deposits generally exhibit three sedimentatry

298   facies: i.e., a carapace facies (the coarsest unit composing the surface and near surface), a body facies (the main

299   body of the rock-avalanche deposit), and a basal facies (the base of the rock-avalanche deposit). The boundary

300   between the basal facies and the body facies is often indistinct in the field. Our MSWA survey showed that these

301   three facies were easily identified from the shear-wave velocity profile (Fig. 10). The carapace and basal facies

302   have smaller shear-wave velocities, while the body facies occupying the main area of the deposits has greater

303   shear-wave velocities. Therefore, the shear-wave velocity profile enables us to not only identify the distribution

304   of these facies, but also to estimate the geotechnical properties of each facies.

305   Hydraulic prediction of downstream flooding due to failure of a landslide dam is of great importance to the

306   assessment of potential damage downstream and effective evacuation. By now, some approaches to this kind of

307 hydraulic prediction have been proposed, based on experimental work on landslide dams consisting of

308 homogenous soil layers. However, as revealed by the grain size distribution of Tianchi landslide dam, a landslide

309 dam normally consists of heterogeneous debris. Therefore, in the analysis of a landslide dam formed by

310 long-runout landslides, the sedimentary facies phenomenon should be considered. Especially in the analysis of

311 breaching risk due to overtopping, the effects of very large boulders in the surficial layers should be taken into

312 account. As in the case of the Tianchi landslide dam, the giant boulders ($\phi=2\sim6m$) of the surficial layer can

313 elevate the resistance to overtopping erosion, and thus retard the occurrence of sudden breaching. On the other

314 hand, as pointed by Dunning and Armitage (2011), the presence of a coarse layer (carapace facies) in the upper

315 part of the landslide dam may enhance permeability, so that the upper layer may become saturated rapidly after

316 overtopping, resulting in rapid breaching. However, the finer materials inside the landslide dam are tightly

317 consolidated and can lower the seepage and lead to a lower water table in the downstream dam body. In this case,

318 even if overtopping occurs, the soil layers in the downstream part of the dam may not be saturated quickly, so

319 collapse failure may not occur.

320 It is noted that at present there is no accepted rapid approach to predict the stability of a landslide dam

321 immediately after its formation. However, we expect that a method combinating the Dimensionless Blockage

322 Index and shear-wave velocity survey results could be developed so that the risk of abrupt breaching of a

323 landslide dam can be assessed rapidly and more reliably. In the future, we plan to carry out similar geophysical

324 surveys on more landslide dams with differing topographic, geological and movement characteristics to develop

325 a physically based method of assessing the breaching risk of landslide dams.

326

327 **6. Conclusions**

328 To understand the formation and mechanisms allowing abrupt breaching of landslide dams that formed

329 during the 2008 Wenchuan ($M_w7.9$) earthquake, a landslide dam that resulted from a long-runout rockslide in the

330 Tianchi area was investigated. Based on geophysical surveys on the dam and grain-size analysis, the internal

331 structure and the stability of this landslide dam were analyzed. The conclusions are as follows:

332   (1) Tianchi landslide resulted from the failure of an unstable rock block in the source area. The displaced

333   landslide mass traveled a long distance, colliding with the opposite river bank, and damming the river. Because

334   the bedding planes and the joints in the source area were well developed, the landslide debris consisted of many

335   very large boulders.

336   (2) Segregation phenomenon occurred within the displaced debris. After a long distance of movement, the

337   larger boulders formed surficial layer, the coarse carapace facies found on many rock avalanche deposits. The

338   debris was much finer deeper within the landslide dam.

339   (3) A seismic geophysical survey of the landslide dam revealed that the soil layers inside the dam had

340   greater shear-wave velocities in general (>330 m/s), and the landslide dam was not homogenous. The surficial

341   layer (carapace facies) and the bottom layer (basal facies) have relatively smaller shear-wave velocities values.

342   Some domains of the central part of the dam also show relatively smaller shear-wave velocities—namely, some

343   relatively weaker layers are sandwiched in the landslide dam.

344   (4) Tianchi landslide dam was covered by huge boulders but consisted of tightly consolidated finer

345   materials. This kind of dam structure can resist overtopping erosion and reduce the likely occurrence of piping,

346   thus retarding breaching immediately after the occurrence of overtopping flow.

347   Last, it is noted that detailed seismic geophysical surveys on many other landslide dams are ongoing to

348   understand the internal structure of landslide dams with differing geological and topographic backgrounds and

349   differing movement mechanisms. The target landslide dams are those triggered by the 2008 Wenchuan

350   earthquake in China, by the 2004 Niigata Prefecture Chuetsu earthquake in Niigata, Japan, and by heavy rainfall

351   during the 2011 Typhoon Talas in Kii Peninsula, Japan. By doing so, we are expecting to enhance the reliability

352   in the analysis of stability of landslide dam with help of shear-wave velocity profiles.

353

363 **References**

364 Burchfiel, B.C., Chen, Z., Liu, Y., Royden, L.H., 1995. Tectonics of the Longmen Shan and adjacent regions,

365   central China, International Geological Review 37, 661–735.

366 Burchfiel, B.C., Royden, L.H., van der Hilst RD, Hager, B.H., 2008. A geological and geophysical context for

367   the Wenchuan earthquake of 12 May 2008, Sichuan, People's Republic of China, GSA Today 18

368 Casagli, N., Ermini, L., 1999. Geomorphic analysis of landslide dams in the northern Apennine. Transactions of

369   the Japanese Geomorphological Union 20, 219– 249.

370 Casagli, N., Ermini, L. Rosati G. 2003. Determining grain size distribution of the material composing landslide

371   dams in the Northern Apennines: sampling and processing methods. Engineering Geology, 69(1-2): 83-97

372 Chigira, M., Wu, X.Y., Inokuchi, T., Wang, G., 2010: Landslides induced by the 2008 Wenchuan earthquake,

373   Sichuan, China. Geomorphology, 118(3-4.: 225-238.

374 Costa, J.E., Schuster, R.L., 1988. The formation and failure of natural dams, Geological Society of America

375   Bulletin 100, pp. 1054–1068

376 Costa, J.E., Schuster, R.L., 1991. Documented historical landslide dams from around the world. U.S. Geological

377   Survey Open-FileReport 91-239, 1-486.

378 Crosta, G.B., Frattini, P., Fusi, N., Sosio, R. 2011. Formation, characterization, and modeling of the Val Pola

379   rock-avalanche dam (Italy). Chapter 12, in Natural and Artificial Rockslide dams (Evans, Hermanns, Strom,

380   and Scarascia-Mugnozza, eds.), Springer, pp:347-368

381 Dai, F.C., Xu, C., Yao, X., Xu, L., Tu, X.B. and Gong, Q.M., 2011. Spatial distribution of landslides triggered by

382   the 2008 Ms 8.0 Wenchuan earthquake, China. Journal of Asian Earth Sciences, 40(4): 883-895

383 Deng Q, Chen S, Zhao X., 1994. Tectonics, seismicity, and dynamics of the Longmen Shan Mountains and its

384   adjacent regions, Seismological Geology 16: 389–403 (in Chinese)

385 Densmore, A.L., Ellis, M.A., Li, Y., Zhou, R., Hancock, G.S., Richardson, N., 2007. Active tectonics of the

386   Beichuan and Pengguan faults at the eastern margin of the Tibetan Plateau, Tectonics 26: TC4005

387 Dunning, S.A., Armitage, P.J., 2011. The grain-size distribution of rock-avalanche deposits: implications for

388   natural dam stability. Chapter 19 in Natural and Artificial Rockslide dams (Evans, Hermanns, Strom, and

389   Scarascia-Mugnozza, eds.), Springer, pp: 497-498.

390 Davies, T.R., McSaveney, M.J., 2011. Rock-avalanche size and runout – implications for landslide dams.

391   Chapter 17 in Natural and Artificial Rockslide dams (Evans, Hermanns, Strom, and Scarascia-Mugnozza,

392   eds.), Springer, pp: 441-462.

393 Ermini, L., Casagli, N., 2003. Prediction of the behaviour of landslide dams using a geomorphological

394   dimensionless index. Earth Surface Processes and Landforms, 28(1): 31-47.

395 Fan, X., Gorum, T., Cees J. van Westen, Korup, O., Xu, Q., Dai, F., Huang, R., Wang, G., 2012. Transient water

396   and sediment storage of the decaying landslide dams induced by the 2008 Wenchuan earthquake, China.

397   Geomorphology 171-172: 58-68.

398 Foster, M.A., Fell, R., Spannangle, M., 2000. The statistics of embankment dam failures and accidents. Canadian

399   Geotechnical Journal 37(5), 1000–1024.

400 Gorum, T., Fan, X.M., van Westen, C.J., Huang, R.Q., Xu, Q., Tang, C., Wang, G., 2011. Distribution pattern of

401   earthquake-induced landslides triggered by the 12 May 2008 Wenchuan earthquake. Geomorphology

402   133(3-4):152-167.

403 Hayashi, K., Suzuki, H., 2004. CMP cross-correlation analysis of multi-channel surface-wave data. Explor.

404   Geophys., 35 (2004), pp. 7–13

405 Huang, R.Q., 2009. Geohazard assessment of the Wenchuan Earthquake. Science Press, 944P (in Chinese)

406 Imai, T., Tonouchi, K., 1982. Correlation of N-value with S-wave velocity and shear modulus. Proc. 2nd

407   European Symp. Of Penetration Testing (Amsterdam), 57–72.

408 Jia, D., Wei, G., Chen, Z., Li, B., Zeng, Q., Yang, G., 2006. Longmen Shan fold-thrust belt and its relation to the

409   western Sichuan Basin in central China: new insights from hydrocarbon exploration, AAPG Bulletin 90:

410   1435–1447.

411   Jia, Q., Jia, D., Zhu, A., Chen, Z., Hu, Q., Luo, L., Zhang, Y., Li, Y. 2007. Active tectonics in the Longmen

412   thrust belt to the eastern Qinghai–Plateau and Sichuan Basin: evidence from topography and seismicity,

413   Chinese Journal of Geology 42: 31–44.

414   Korup, O., 2002. Recent research on landslide dams - a literature review with special attention to New Zealand,

415   Progress in Physical Geography 26, 206-235.

416   Korup, O., 2004. Geomorphometric characteristics of New Zealand landslide dams. Engineering Geology 73,

417   13–35

418   Li, H., Fu, X., Van Der Woerd, J., Si, J., Wang, Z., Hou, L., Qiu, Z., Li, N., Wu, F., Xu, Z., Tapponnier, P., 2008.

419   Co-seismic surface rupture and dextral-slip oblique thrusting of the Ms 8.9 Wenchuan Earthquake. Acta

420   Geologica Sinica 82, 1623–1643.

421   Li, T., Schuster, R.L., Wu, J., 1986. Landslide dams in south central China. In: Schuster, R.L. (Ed.), Landslide

422   Dams Processes, Risk and Mitigation, Special Publication vol. 3. ASCE, pp. 146– 162.

423   Liu, N., 2008. Lesson from the countermeasures on lowering the risk of the dammed lakes formed by large

424   landslides during the 2008 Wenchuan earthquake. Journal of China Water Resources 16,1-7 (in Chinese)

425   Liu N., Zhang J.X., Lin, W., Cheng W.Y., Chen Z.Y., 2009. Draining Tangjiashan barrier lake after Wenchuan

426   earthquake and the flood propagation after the dam break. Science in China Series E: Technological

427   Sciences, 52(4): 801-809.

428   Li, X., Zhou, Z., Yu, H., Wen, R., Lu, D., Huang, M., Zhou, Y., Cu, J., 2008. Strong motion observations and

429   recordings from the great Wenchuan Earthquake. Earthquake Engineering and Engineering Vibration 7,

430   235–246.

431   Ma LF (ed.). 2002. Geological atlas of China, Geological Publishing House, 348p

432   Mizuyama, T., Ishikawa, Y., Fukumoto, A., 1987. Landslide dams outburst due to seepage. Annual of Public

433   Works Research Institute, Vol.2744, 18-91 (in Japanese).

434   Mizuyama, T., Ishikawa, Y., Fukumoto, A., 1989. Landslide dams outburst and its Countermeasure. Civil

435   Engineering Journal, Vol.31-11; 50-56 (in Japanese).

436   Park, C.B., Miller, R.D., Xia, J., 1999. Multichannel analysis of surface waves. Geophysics, 64 (3), 800–808.

437   Schulz, W.H., Harp, E.L., Jibson, R.W., 2008. Characteristics of large rock avalanches triggered by the

438   November 3, 2002 Denali Fault earthquake, Alaska, USA, Proc. 10th ISL, Xian, China, June 30-July 4, 2008,

439   Taylor and Francis Group, London, 1447-1453.

440   Sherard, J.L., 1979. Sinkholes in dams of coarse, broadly graded soils, 13th ICOLD Congress, India, Vol. II, pp.

441   25-35.

442   Strom, A., 2010. Landslide dams in Central Asia region. Journal of the Japan Landslide Society 47(6), 309-324.

443   Tabatake, S., Mizuyama T., Inoue, K., 2002. Landslide dam and hazards, Kokon Press, 205pp.

444   Takahashi, T., Kuang, S.F., 1988. Hydrograph prediction of debris flow due to failure of landslide dam. Annuals,

445   Disas. Prev. Res. Inst., Kyoto Univ., No.31 B-2: 601-615.

446   Takahashi, T., Nakawaga H., 1993. Flood and Debris flow hydrograph due to collapse of a natural dam by

447   overtopping. Journal of Hydroscience and Hydraulic Engineering, JSCE, 37: 699-704.

448   USGS, 2008. Website (http://earthquake.usgs.gov/eqcenter/eqinthenews/2008/us2008ryan/), accessed on

449   September 17, 2012.

450   Wang, G., 2011. Formation of large scale landslide dams and failure prediction. Proceedings of 2011 landslide

451   symposium, Kansai Branch of Japan Landslide Society, pp:65-80 (in Japanese).

452   Wang, Q., Wang, Y.S., Jiang, Y.A., Wei, P., Zhi, Z.Z., 2011. The initiation mechanism and movement process of

453   Tianchi landslide. Gansu Water Conservancy and Hydropower Technology 47(1):16-18 (In Chinese).

454   Xu, Q., Fan, X.M., Huang, R.Q., Van Westen, C.J., 2009. Landslide dams triggered by the Wenchuan Earthquake,

455   Sichuan Province, south west China. Bull Eng Geol Environ 68:373-386.

456   Yin, Y.P., 2008. Researches on the Geo-hazards triggered by Wenchuan Earthquake, Sichuan, Journal of

457   Engineering Geology 16: 433-444 (in Chinese).

458   Zhu, P.Y., Wang, C.H., Wang Y.C., 2003. Large-scale landslide-debris avalanche in Tibet, China, (2) formation

459   of an exceptionally serious outburst flood from a landslide dam in Tibet. Landslide News, International

460   newsletter of the Japan Landslide Society, 14/15: 23-25.

461 **Captions:**

462 Fig. 1 Epicenter of the Sichuan earthquake, the distribution of landslides, and location of the Tianchi landslide

463 dam (after Huang and Li, 2009).

464

465 Fig. 2 Landslide dam in the Tianchi area: (a) satellite image of landslide area before the quake; (b) view of the

466 landslide from upstream of the dam after channel excavation (taken on March 19, 2011); (c) landslide dam and

467 lake (Courtesy of F. Cai, taken on November 7, 2008 by F. Cai); (d) landslide dam viewed from downstream

468 (Courtesy of F. Cai, taken on November 7, 2008)

469

470 Fig.3   Geological settings of the Tianchi area – 1: Stratum boundary; 2: Fault; 3: Tianchi landslide area; 4:

471 Quaternary alluvial and diluvial deposit; 5: Triassic sandstone, conglomerate, siltstone and mudstone; 6:

472 Triassic shale; 7: Triassic clastic rock and carbonate rock; 8: Permian shale, limestone and basalt; 9: Devonian

473 sandstone and conglomerate with carbonate rock; 10: Devonian clastic rock and carbonate rock; 11: Silurian

474 slate; 12: Cambrian shale, siltstone, mudstone and sandstone; 13: Cambrian dolomite; 14: Sinian dolomite and

475 marble; 15: Proterozoic acid volcanic, clastic rock and carbonate rock; 16: Proterozoic granite; 17: Diabase

476 dike (after Ma, 2002)

477

478 Fig. 4 (a) Source area of the landslide; (b) Stereonet plot of rock-mass discontinuities in the source area

479

480 Fig. 5 Longitudinal section along line I-I' in Fig. 2a

481

482 Fig. 6 (a) Photograph of landslide dam after excavation, with locations of shear-wave velocity survey lines and
483 grain-size sampling points (P1–P11); (b) Cross section of the landslide dam at differing surveying times. L3,
484 L4: spillway levels on November 20, 2009, and June 16, 2010, respectively.

485

486 Fig. 7 Grain size distributions of materials from dam body: (a) samples on the same altitude level, (b) samples at

487 different depths within the dam body

488
489 Fig. 8 Measurement principle of multichannel analysis of surface waves (MASW).
490

491   Fig. 9 Shear-wave velocity profile along traverse line L1

492

493   Fig. 10 Shear-wave velocity profile of the dam body. (a), (b), (c): results for traverse line L2, L3 and L4,

494   respectively

495

496   Fig.11 Stability analysis using Dimensionless Blockage Index (after Ermini and Casagli (2003)) ▲ : intact

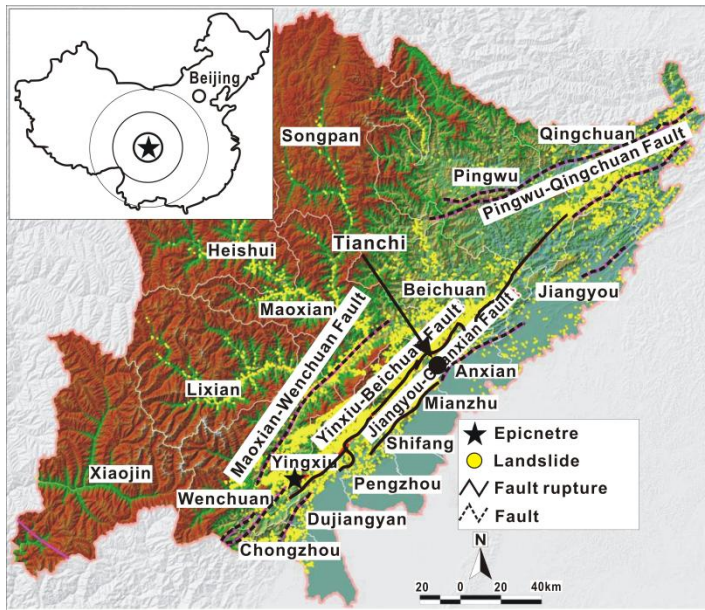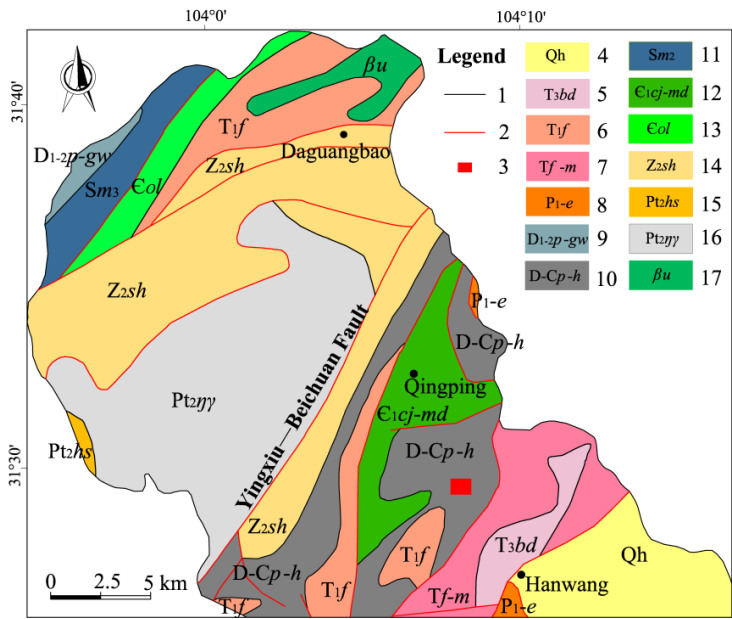497   landslide dams; ◆:collapsed landslide dams

498   Figures

512   Fig. 1 Epicenter of Sichuan earthquake, distribution of landslides, and location of Tianchi landslide dam (after

513   Huang and Li (2009)).

532   Fig. 2 Landslide dam in Tianchi area. (a) aerial photo of landslide area before the quake; (b) View of the

533   landslide from the upper stream of the river after all construction has been finished (Taken on March 19,

534   2011); (c) Landslide dam and lake (Courtesy of F. Cai, taken on November 7, 2008 by F. Cai) viewing from

535   upstream; (d):Landslide dam viewing from downstream (Courtesy of F. Cai, taken on November 7, 2008)

536
537
538
539
540
541
542
543
544
545
546
547
548
549
550
551
552
553
554
555
556

557   Fig. 3   Geological settings of Tianchi area (1: Stratum boundary; 2: Fault; 3: Tianchi landslide area; 4:

558   Quaternary alluvial and diluvial deposit; 5: Triassic Sand, conglomerate, siltstone and mudstone; 6: Triassic

559   shale; 7: Triassic clastic rock and carbonate rock; 8: Permian shale, limestone and basalt; 9: Devonian

560   sandstone and conglomerate with carbonate rock; 10: Devonian clastic rock and carbonate rock; 11: Silurian

561   slate; 12: Cambrian shale, siltstone, mudstone and sandstone; 13: Cambrian dolomite; 14: Sinian dolomite and

562   marble; 15: Proterozoic acid volcanic, clastic rock and carbonate rock; 16: Proterozoic granite; 17: Diabase

563   dike)(after Ma, 2002)

564
565
566
567
568
569
570
571
572
573
574
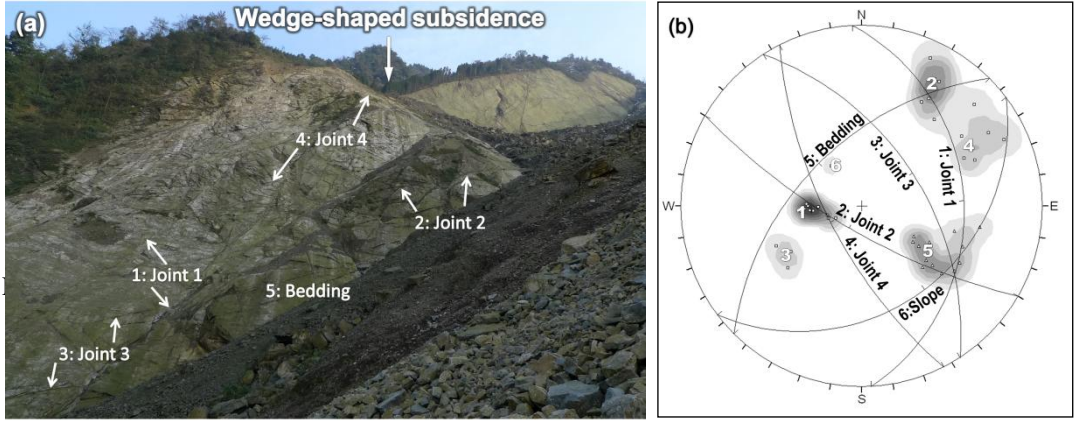
575   Fig. 4 (a): Source area of the landslide, (b): Stereonet graph of the discontinuities of rocks on the source area
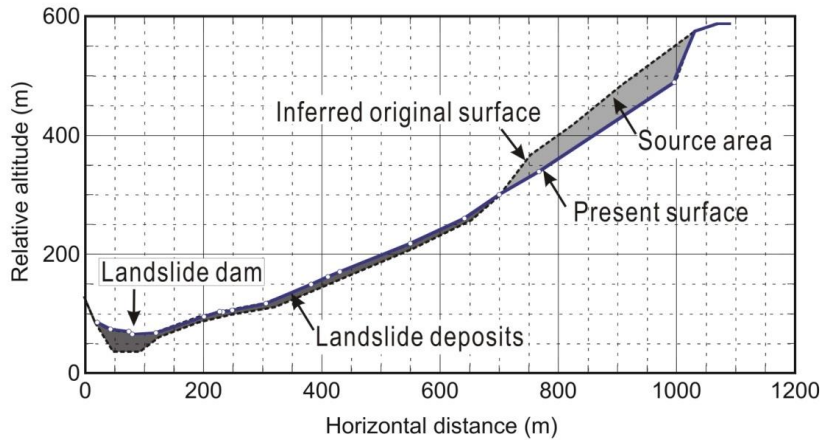
Fig. 5 Longitudinal section along line I-I' in Photo 2a
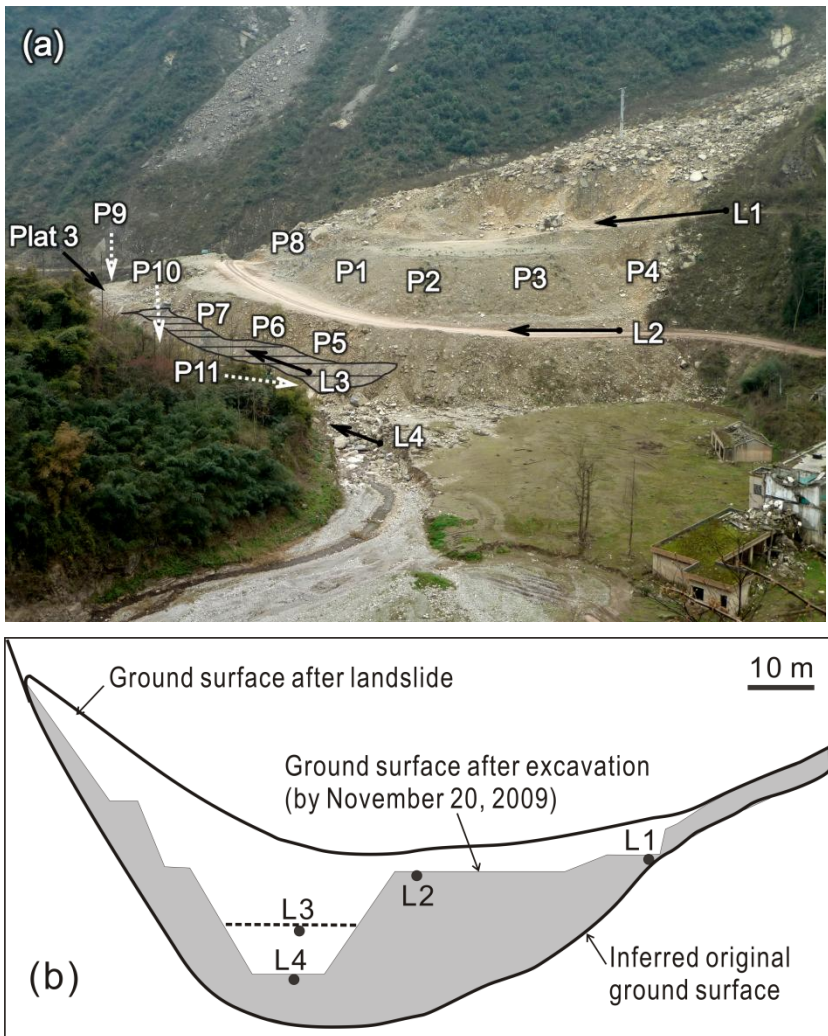
Fig. 6 (a) Photo of landslide dam after excavation with locations of S-wave survey lines and grain size analysis
points (P1~P11); (b) Cross section of the landslide dam during differing surveying times. L3, L4: spillway
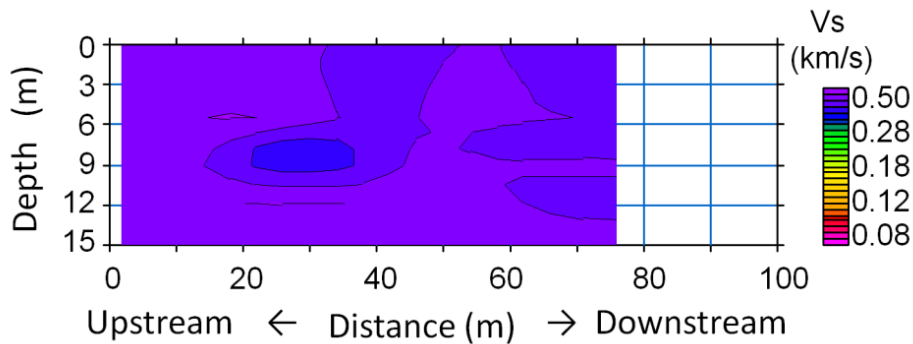levels on November 20, 2009, and June 16, 2010, respectively.
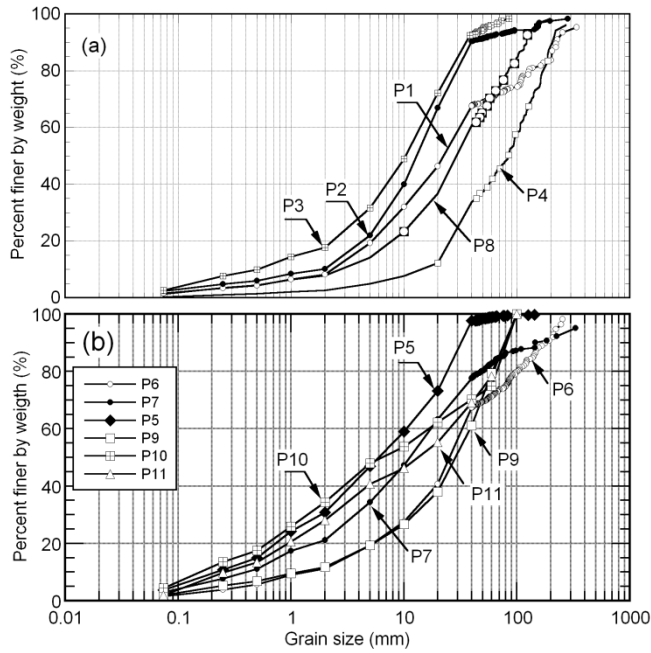
Fig. 7 Grain size distributions of materials from dam body. (a): samples on the same altitude level. (b): Samples at different depth of the dam body
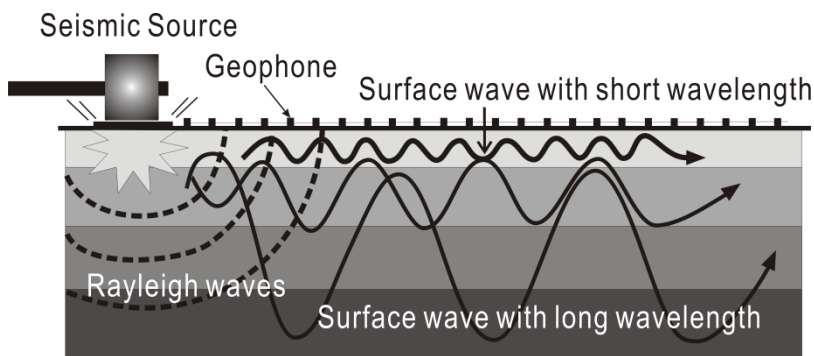
Fig. 8 Measurement principle of multichannel analysis of surface waves (MASW).
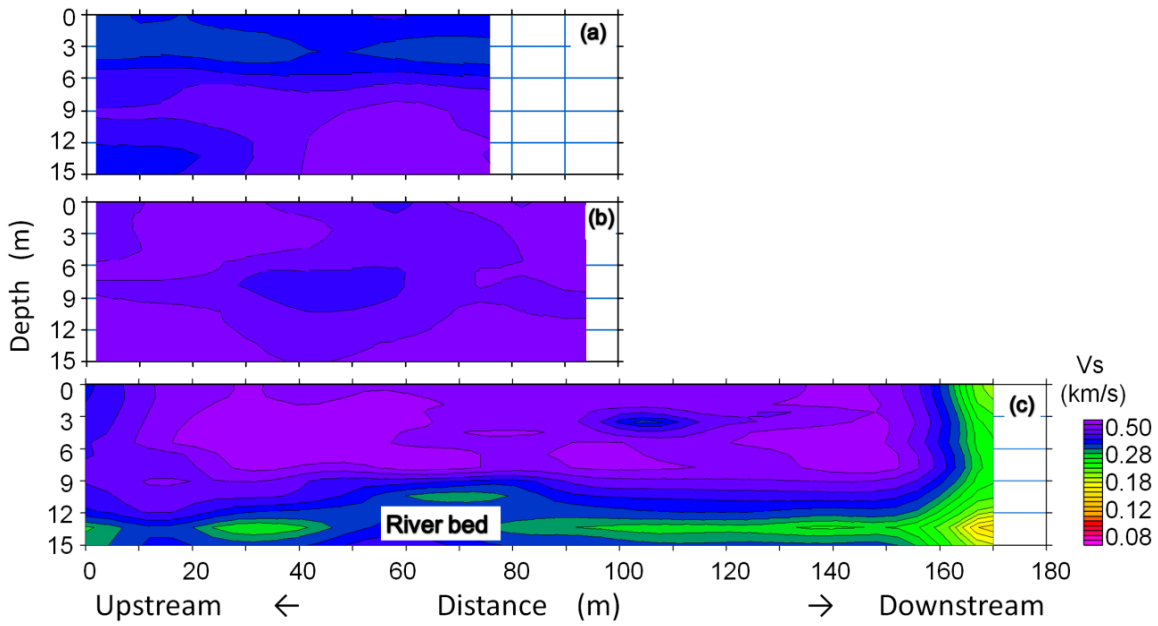

Fig. 9 Shear-wave velocity (Vs) profile along traverse line L1

677

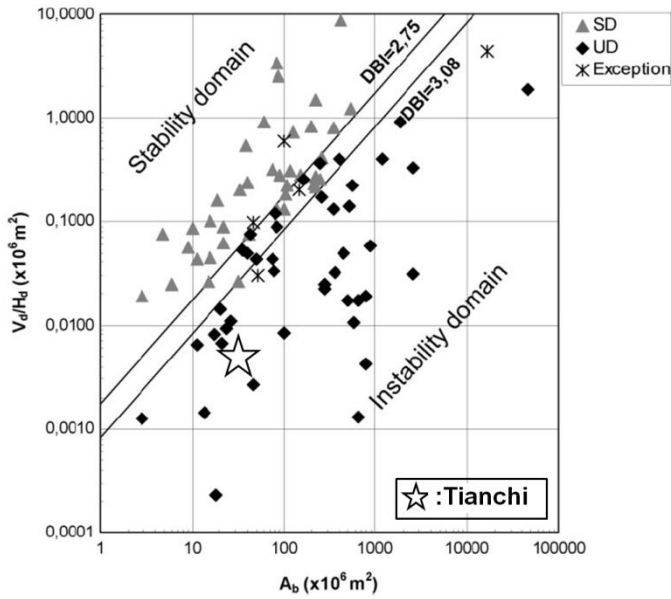Fig. 10 Shear-wave velocity (Vs) profile of the dam body. (a), (b), (c): results for traverse line L2, L3 and L4, respectively

Fig.11 Stability analysis using Dimensionless Blockage Index (after Ermini and Casagli (2003)) ▲ : intact landslide dams; ◆: collapsed landslide dams